Journal of Sound and Vibration 352 (2015) 192–209

Contents lists available at ScienceDirect

Journal of Sound and Vibration

journal homepage: www.elsevier.com/locate/jsvi

A transient tribodynamic approach for the calculation of internal combustion engine piston slap noise

N. Dolatabadi, B. Littlefair, M. De la Cruz, S. Theodossiades *,[1], S.J. Rothberg, H. Rahnejat

Wolfson School of Mechanical and Manufacturing Engineering, Loughborough University, Loughborough LE11 3TU, UK

ARTICLE INFO

Article history:
Received 13 November 2014
Received in revised form
24 March 2015
Accepted 15 April 2015
Handling Editor: P. Joseph
Available online 27 May 2015

ABSTRACT

An analytical/numerical methodology is presented to calculate the radiated noise due to internal combustion engine piston impacts on the cylinder liner through a film of lubricant. Both quasi-static and transient dynamic analyses coupled with impact elasto-hydrodynamics are reported. The local impact impedance is calculated, as well as the transferred energy onto the cylinder liner. The simulations are verified against experimental results for different engine operating conditions and for noise levels calculated in the vicinity of the engine block. Continuous wavelet signal processing is performed to identify the occurrence of piston slap noise events and their spectral content, showing good conformance between the predictions and experimentally acquired signals.

1. Introduction

Internal combustion (IC) engines have been extensively deployed in various configurations for transportation (vehicles, ships, motorcycles etc.). There have been ever increasing concerns with regard to their radiated noise levels, fuel consumption and emissions. These concerns, together with the growing competition have forced industry to increase investment in research and development. As the parasitic losses of piston – cylinder system account for 6–9 percent of fuel consumption [1], including friction and errant dynamics, their investigation has been regarded as beneficial.

One effect of errant dynamic behaviour is the induced noise, which is regarded as a sign of poor quality. Piston slap due to secondary piston inertial dynamics is one such noise propagating concern. The generated noise is due to piston impact on the cylinder liner, which has been a problem for the research community for a long time. The noise generation mechanism can be analysed in three phases: (i) vibration excitation at the source, (ii) energy transfer through a structural path and (iii) noise radiation from the vibrating surfaces [2]. In vehicular powertrains, noise can originate from processes and associated components, such as combustion, piston slap, fuel injection, gear teeth contacts, oil pump and valve impacts. Fig. 1 shows the contributions to the total engine noise levels from the aforementioned noise sources for a three-cylinder,

Abbreviations: ATS, Anti-thrust side; ABDC, After bottom dead centre; ATDC, After top dead centre; BDC, Bottom dead centre; BBDC, Before bottom dead centre; BTDC, Before top dead centre; COG, Centre of gravity; CWS, Continuous wavelet spectrum; EHL, Elasto-hydrodynamic lubrication; EVC, Exhaust valve closure; EVO, Exhaust valve opening; IVC, Inlet valve closure; IVO, Inlet valve opening; NVH, Noise, Vibration and Harshness; SPL, Sound pressure level; SPL_T, Total sound pressure level; TDC, Top dead centre; TS, Thrust side

* Corresponding author.
E-mail address: S.Theodossiades@lboro.ac.uk (S. Theodossiades).

[1] Research data for this paper are available on request from Dr. Stephanos Theodossiades (S.Theodossiades@lboro.ac.uk).

http://dx.doi.org/10.1016/j.jsv.2015.04.014
0022-460X/

List of symbols

A_r	surface area of noise radiating source
A_v	surface area of impacted structure
a	distance between the pin-bore and top of piston skirt
b	distance between the piston centre of gravity and top of piston skirt
C	nominal clearance between piston and cylinder liner
c_a	wave propagation speed in air
d	combined effect of instantaneous clearances; e_t and e_b
d_{COG}	offset between the piston centre of gravity and the pin-bore
d_p	offset between point of action of gas force and the pin-bore
e_b	eccentricity at the bottom of piston skirt
e_t	eccentricity at the top of piston skirt
$\overline{F}$	average lubricant reaction between two consecutive time steps
F_f	piston – cylinder conjunctional friction
F_G	gas force
F_{hyd}	lubricant reaction
F_L	connecting rod force
$F_{pin,x}$	pin reaction along the x coordinate
$F_{pin,z}$	pin reaction along the z coordinate
F_t	lateral (side) force acting on the piston
h	lubricant film thickness
h_t	thickness of the structure
I_{pis}	piston inertia
L	piston skirt height
L_w	sound power level
M_f	viscous friction moment
M_{hyd}	viscous reaction moment due to load
M_s	tilting moment due to pin or crankshaft offset
m_{pin}	mass of piston pin
m_{pis}	mass of piston
P	elasto-hydrodynamic pressure
P_a	acoustic power
P_{ref}	reference acoustic power
P_v	impact power
R	radius of piston crown
R_b	distance from the block surface
r	piston profile
S	overall skirt deformation
$\bar{s}_0$	acoustic field characteristic
t	time
U_{av}	speed of entraining motion of the lubricant
V_{av}	lubricant side leakage velocity
v	lubricant film squeeze velocity
v_r	surface vibration velocity
v_v	impact velocity
W	transferred energy
x	coordinate along the axis of the cylinder
Y	impact mobility
Z	impact impedance
z	coordinate transverse to the axis of the cylinder

Greek letters

η	lubricant dynamic viscosity
$\eta_{a/v}$	structural attenuation ratio
η_0	atmospheric dynamic viscosity of the lubricant
Θ	lubricant temperature
Θ_0	bulk oil temperature
θ	crank angle
ρ	lubricant density
ρ_a	density of air
ρ_v	density of the impacted structure
ρ_0	atmospheric density of lubricant
σ	surface radiation efficiency
ϕ	connecting rod obliquity angle

water-cooled gasoline engine at a speed of 2500 rpm [2]. As can be seen, combustion and piston slaps are significant contributors with their cumulative share representing about 80 percent of the total engine noise output [2]. Piston slap represents the most significant mechanical noise source, comparable with the combustion-induced noise [2–4].

Piston slap occurs due to the differing load conditions between the piston skirt and the cylinder wall. The type of contact is determined by the regime of lubrication, which can be hydrodynamic, elastohydrodynamic, mixed, or even boundary, depending on the prevailing kinematics/loading, geometry and lubricant rheological state [5]. The noise transfer mechanism from the piston assembly to the surface of the engine block is shown in Fig. 2. Piston slap depends on the variations of the cylinder pressure and the inertia of the piston assembly. The vibrations generated reach the engine block through the cylinder liner. Surface vibrations of the block induce sound propagation into the environment. The forces acting on the piston assembly originate from three main sources: (a)- the cylinder pressure, (b)- component inertia and (c)- the lubricant film. Numerous studies have been reported in modelling the cylinder pressure analytically [6,7], whilst this is commonly measured for piston-slap investigations [3,8,9]. Models describing piston dynamics usually exclude its tilting motion through piston pin rotation [10,11] or simply use constrained Lagrangian dynamics to include the component reactions due to piston rotation [8,12]. Methodologies involving multibody dynamics and Finite Element Analysis (FEA) software, such as MSC ADAMS and NASTRAN, have been reported for the study of piston secondary motion [13–16].

In earlier studies of piston dynamics, the effects of lubrication were generally neglected [10,11]. Later, a coefficient of friction was included in the equations of motion to account for the frictional losses [17]. In order to add the effect of lubricant film damping, spring-damper arrangements in parallel and/or in series have been considered [12,18–20]. A more accurate representation of lubricant behaviour is obtained through the solution of Reynolds equations [15,16, 21]. Cho and

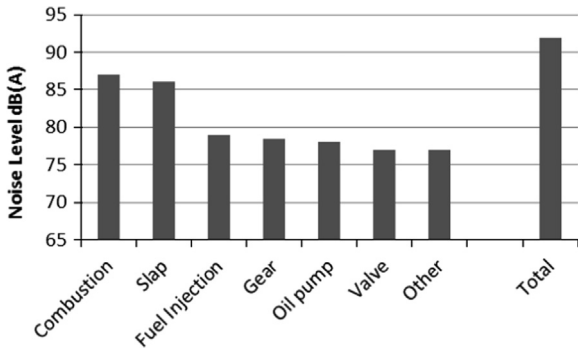

Fig. 1. Indicative noise contributions in a three-cylinder water-cooled gasoline engine [2].

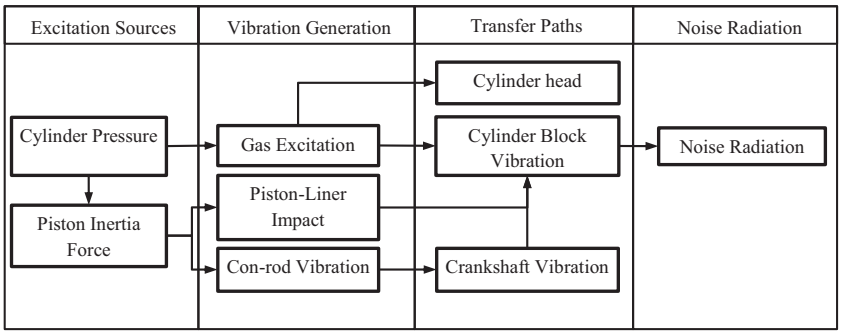

Fig. 2. Noise generation and transfer paths in an IC engine.

Moon [22] studied the conjunctional lubricant behaviour using a quasi-static approach, in which piston tilting motion was taken into account, but the effect of lubricant squeeze velocity was neglected. McClure investigated the contact conditions between the piston and the cylinder bore using a transient approach, including the thermo-elastic distortion of piston skirt [23]. In the transient solution of conjunctional pressure and film thickness, the squeeze action of the oil film was included. D'Agostino et al. [8] and Littlefair et al. [24] considered the piston-skirt deformation when estimating the oil film thickness, with the latter demonstrating very good agreement between the numerical predictions and ultrasonically measured lubricant film thickness. They have all combined the oil film behaviour with piston dynamics (tribo-dynamics), forming a multi-physics study of the piston's secondary motion. Further studies have been reported with the variations in the lubrication regime during the full engine cycle taken into account, together with the piston-profile and the connecting rod effects [6,8,23–25].

The above mentioned piston-liner contact tribo-dynamic models are employed to identify piston slap events, irrespective of the structural excitation, engine block response and sound quality (dB levels and frequency) perceived by the receiver [26]. In tribo-dynamics, the effect of sound power structural attenuation has been investigated for the cylinder liner and the engine block through modal analysis [18,20]. Structural analysis has been reported using FEA [14,22]. A direct relationship was established between the vibration levels of the engine block and the excitation force/surface velocities at the impact sites of the cylinder liner's inner surface [11,12]. The impact impedance has been used at each contact point between the piston and the cylinder liner in order to predict the surface vibrations of the engine block. In some practical approaches, a transfer function has been established experimentally to describe the noise attenuation characteristics through the engine block [9,19].

The current study presents the development of a novel numerical/analytical method to investigate internal combustion engine NVH with the main emphasis placed on the identification of piston slap events. The prediction of noise levels, impact characteristics and structural analysis of the engine block are the objectives, whereas in the authors' previous paper [26] the focus was mainly on the number and location of events during the internal combustion engine cycle. The novel contribution of this paper lies in the integration of impact in elastohydrodynamic lubrication (EHL) with piston transient dynamics in order to identify potential slap noise events. In this multi-physics framework, the conjunctional pressures generated and the oil film thickness variations are used to estimate the impact force and the squeeze film velocity. The localised impact impedance is calculated to determine the energy transferred to the structure and successively to estimate the structural attenuation factor used in the prediction of the sound power loss through the cylinder-block structure. The piston secondary motion is correlated to the surface vibrations of the engine block and the latter are then used to calculate the radiated noise

levels. The sound levels predicted by this method are suitable for comparison with experimentally measured noise levels and quantification of the user/receiver's perception of noise at any location of interest from the engine. The methodology is validated against experimental measurements obtained from a single-cylinder Honda CRF 450 motocross motorbike high performance normally aspirated gasoline engine. The good correlation between the numerical and experimental results verifies the developed method.

2. Piston dynamics

Fig. 3a shows the primary (axially reciprocating) and secondary (lateral and tilting) motions of the piston within the cylinder liner. Piston dynamics are commonly defined by piston eccentricities from its aligned orientation at the top and bottom of the skirt (e_t and e_b), resulting from its secondary motion [5,21]. Piston eccentricities e_t, e_b are piston displacements from the centre-line of cylinder liner. L and R are the skirt length and piston crown radius, respectively. θ is the crank angle, commencing from the top dead centre (TDC). The two sides of the cylinder wall are commonly referred as *TS* (thrust side) and *ATS* (anti-thrust side). In the combustion stroke, the piston initially impinges onto the thrust side of the liner.

Fig. 3a and b depicts the piston and pin free body diagrams. m_{pis}, m_{pin} and I_{pis} are the piston mass, pin mass and piston centroidal moment of inertia. The centre of gravity and excitation force offsets are at distances d_{COG} and d_p in the lateral direction with respect to the piston's centre-line and at distances b and a in the primary axial direction with respect to the upper surface of the skirt. ϕ is the connecting rod angle with respect to the cylinder axis. Inertial forces are represented by $m_{\text{pis}}\ddot{x}$, $m_{\text{pis}}\ddot{z}$ for the piston and $m_{\text{pin}}\ddot{x}$, $m_{\text{pin}}\ddot{z}$ for the pin, respectively. Other forces in Fig. 3b are: the combustion force F_G, the lubricant reaction $F_{\text{hyd}} = \iint P\mathrm{d}x\mathrm{d}z$, the oil film viscous friction force F_f, the connecting rod force F_L and the pin reaction forces $F_{\text{pin},x}$ and $F_{\text{pin},z}$.

The secondary piston motion is related to its primary dynamics. This can be established in one of two alternative approaches: (i) a purely kinematic analysis or (ii) including inertial dynamics. In the former approach, the piston secondary motion and the lubricant film load carrying capacity are ignored, when estimating the primary force. In the latter approach (inertial dynamics) these effects are considered. Thus, in the kinematics approach, the lateral resultant force acting on the

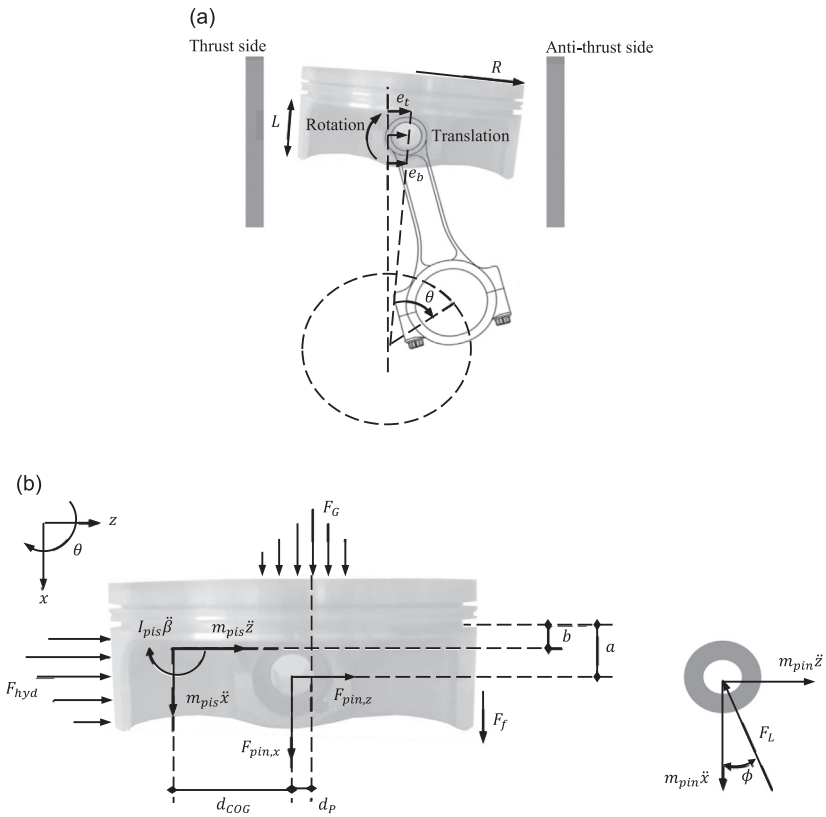

Fig. 3. (a) Piston secondary motions; (b) Piston and pin free-body diagrams.

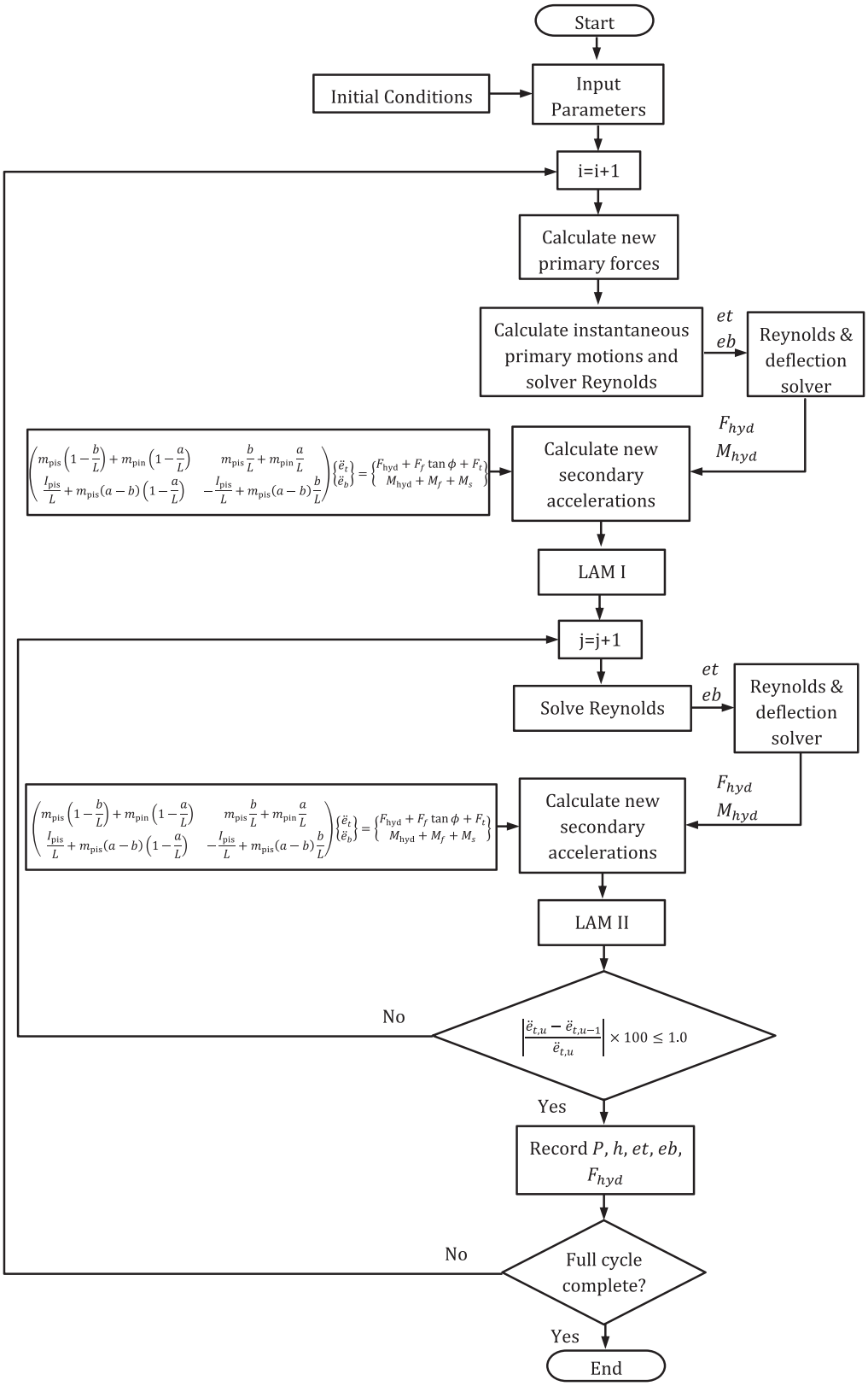

Fig. 4. The flow chart for the transient dynamic model.

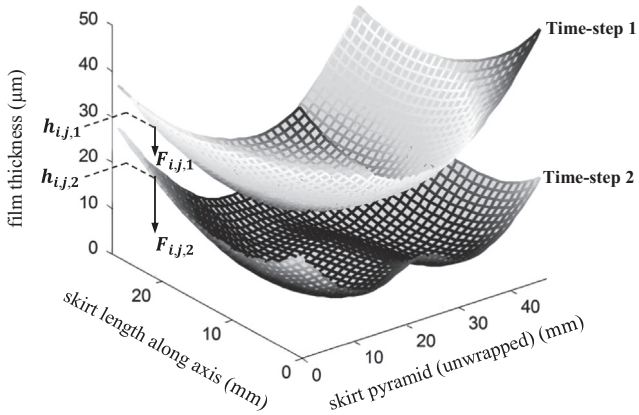

Fig. 5. Film shape at time steps 1 and 2. Force and film thickness indicators at an arbitrary point (i,j) on the piston skirt are shown to represent the energy calculation.

piston, F_t, can be calculated using the forces in the primary axial direction as:

$$F_t = (F_G + m_{\text{pis}}\ddot{x} + m_{\text{pin}}\ddot{x} + F_f)\tan\phi \tag{1}$$

In order to include the effect of piston secondary motion and lubricant reaction using inertial dynamics, the set of equations of motion (2) is iteratively solved, simultaneously with Reynolds equation [21,25]. Thus, the lateral force is obtained in a more realistic manner. The deviation between the results of methods (i) and (ii), when predicting the lateral force, is quite small at lower engine speeds. As the piston speed increases and inertial effects become significant, the aforementioned methods yield divergent results. The evaluated lateral force from Eq. (2) is used hereinafter to calculate the lateral impact force and approach velocity.

$$\begin{pmatrix} m_{\text{pis}}(1-\frac{b}{L}) + m_{\text{pin}}(1-\frac{a}{L}) & m_{\text{pis}}\frac{b}{L} + m_{\text{pin}}\frac{a}{L} \\ \frac{I_{\text{pis}}}{L} + m_{\text{pis}}(a-b)(1-\frac{a}{L}) & -\frac{I_{\text{pis}}}{L} + m_{\text{pis}}(a-b)\frac{b}{L} \end{pmatrix} \begin{Bmatrix} \ddot{e}_t \\ \ddot{e}_b \end{Bmatrix} = \begin{Bmatrix} F_{\text{hyd}} + F_f \tan\phi + F_t \\ M_{\text{hyd}} + M_f + M_s \end{Bmatrix} \tag{2}$$

M_{hyd} is the moment due to load capacity variation of the lubricant film F_{hyd} over the piston skirt area. M_f is the moment due to the viscous friction of the lubricant film F_f. M_s represents the tilting moment due to pin or crankshaft offset, which equates to: $F_G d_p - m_{\text{pis}}\ddot{x}d_{\text{COG}}$. It should be noted that the lubricant viscous friction and its generated moment are neglected in the current study as their influence on the impact force is quite small, constituting less than 3 percent of the total impact force [27].

The flow chart for the iterative solution of the equations of motion is presented in Fig. 4. LAM I and LAM II are the predictor and corrector routines for the numerical solution. The simulation time corresponds to three engine cycles under all the operational conditions (sufficient to achieve steady state motion per engine cycle). The time step is fixed at 5 μs. The limit of convergence is set to 1 percent tolerance and applied accelerations of piston top and bottom surfaces (i.e. $\ddot{e}_t$ and $\ddot{e}_b$), which are the fastest changing system variables.

3. Effect of lubricant film

To include the effect of lubricated contact, the solution of Reynolds equation is required, with its general form being:

$$\frac{\partial}{\partial x}\left(\frac{\rho h^3}{\eta}\frac{\partial P}{\partial x}\right) + \frac{\partial}{\partial y}\left(\frac{\rho h^3}{\eta}\frac{\partial P}{\partial y}\right) = 12\left\{U_{\text{av}}\frac{\partial}{\partial x}(\rho h) + V_{\text{av}}\frac{\partial}{\partial y}(\rho h) + \frac{\mathrm{d}}{\mathrm{d}t}(\rho h)\right\} \tag{3}$$

where x is the direction of lubricant entrainment along the axial direction of the cylinder liner and y is the circumferential direction (if viewed as unwrapped). P and h are the generated pressure and lubricant film thickness, respectively. The lubricant density, ρ, is a function of pressure [28].

$$\rho = \rho_0\left(1 + \frac{0.6\times10^{-9}\times P}{1 + 1.7\times10^{-9}\times P}\right) \tag{4}$$

ρ_0 is the atmospheric density at the average measured liner temperature. The liner temperature is chosen because a recent thermo-hydrodynamics numerical analysis by Morris et al. [29], using a control volume thermal-mixing method has shown that the lubricant film temperature remains close to that of the liner surface, with only a small rise due to its viscous shear compared with the surface temperature. The lubricant viscosity, η, is also a function of pressure and temperature, where η_0 is the lubricant atmospheric dynamic viscosity at the measured liner temperature. The viscosity variation with pressure is

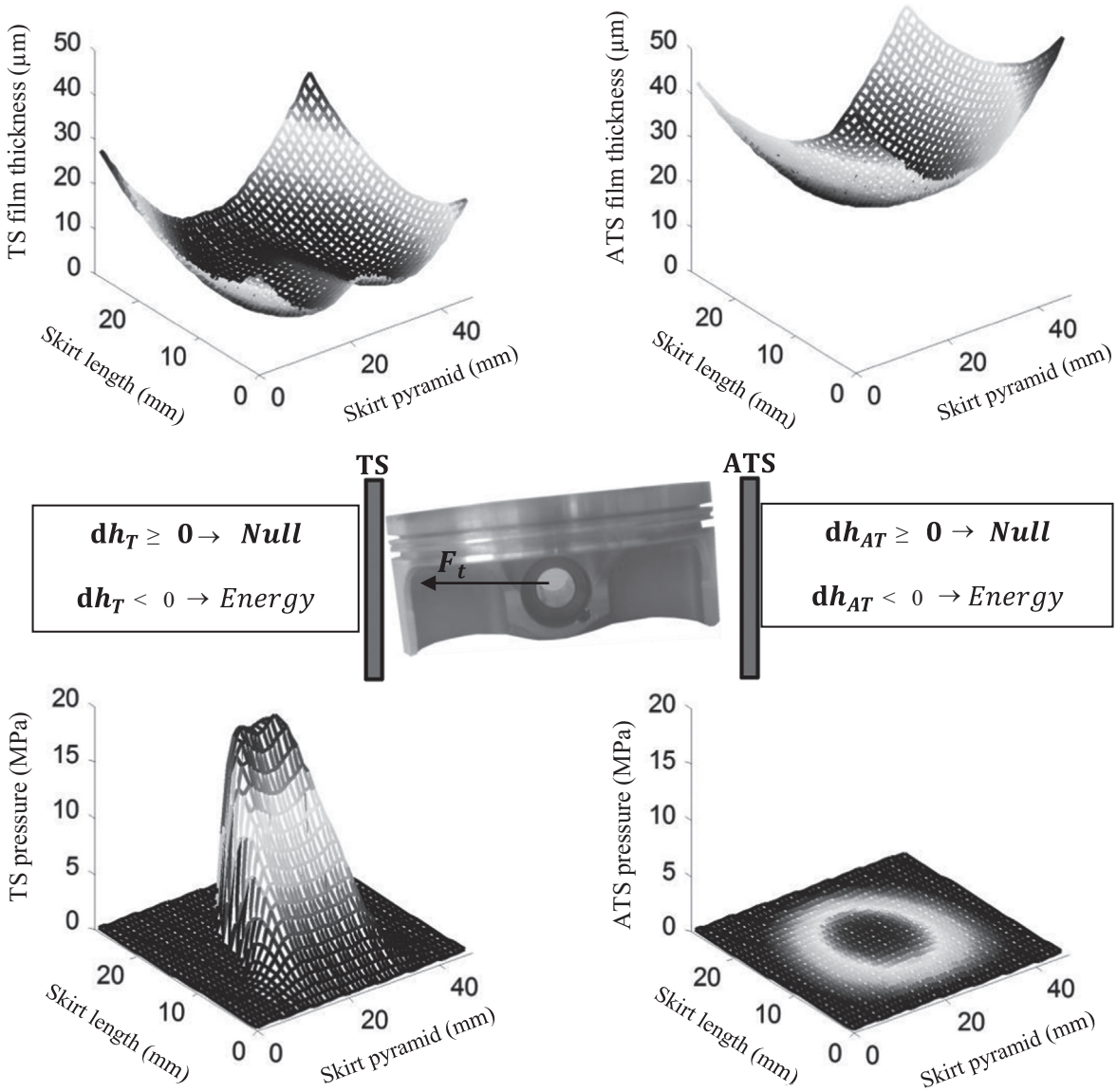

Fig. 6. Calculation of impact energy at the TS and ATS.

given by Roeland [30]:

$$\eta = \eta_0 e^{\alpha} \tag{5}$$

where

$$\alpha = \frac{1}{P}(\ln \eta_0 + 9.67)\left\{\left(\frac{\Theta - 138}{\Theta_0 - 138}\right)^{-S_0}\left(1 + \frac{P}{1.98 \times 10^8}\right)^{Z} - 1\right\}$$

S_0 and Z are constants, independent of temperature and pressure. Θ is the temperature (in K). Θ_0 is the bulk oil temperature. U_{av} is the speed of entraining motion of the lubricant (half the piston sliding velocity). No side leakage flow is assumed ($V_{av} = 0$). Therefore, the second term on the right hand side of Eq. (3) is omitted from the computations. The Reynolds equation can be solved in two different ways: (i)- quasi-static and (ii)- transient. In a quasi-static solution, the lubricant film time history is ignored (the third term on the right-hand side of Eq. (3) is omitted). In a transient solution, the time history of the lubricant film thickness is retained. The instantaneous skirt profile and stiffness are updated in the film thickness estimation at each time step (corresponding to a given crank angle position), using Eq. (6). Here, C is the nominal clearance between the piston and the cylinder liner surface, $r(x, y)$ is the piston profile, $d(x, y, t)$ represents the combined effect of the instantaneous clearances e_t and e_b (which are outputs of the system dynamics) and $S(x, y, t)$ indicates the overall skirt deflection [23–25]. In a quasi-static solution, the term $d(x, y, t)$ is also neglected, as piston dynamics are not taken into

account.

$$h(x,y) = C + r(x,y) + \mathrm{d}(x,y,t) + S(x,y,t) \tag{6}$$

4. Local impact energy

The advantage of employing energy-based methods is the adherence to the principle of conservation of energy through the impact process [31]. Previous piston slap research has either excluded the role of lubricated impact or employed spring-damper lumped parameter models for the energy transfer mechanisms [12]. In the current study, an EHL solution is utilised for the calculation of the transferred energy through the lubricant film caused by the piston secondary motion. Additionally, piston skirt deformation effects are considered, thus reducing the transferred energy (as some of the impact energy is consumed in localised deformation). Impact impedance calculations are then applied to the energy distribution across the discretised piston skirt in order to estimate the energy transferred to the cylinder liner.

The tribodynamic equations provide the lubricant film shape and the generated contact pressure distribution acting on the skirt area at each time step (crank angle position). The parameters affecting the transferred energy through the lubricant film are illustrated in Fig. 5. $F_{i,j,1}$ and $h_{i,j,1}$ are the lubricant hydrodynamic force and film thickness at a grid point (i,j) of the skirt during time step 1, whilst $F_{i,j,2}$ and $h_{i,j,2}$ pertain to the same grid point (i,j) during time step 2. The contact force (lubricant reaction) is the integrated pressure (P) over the elemental grid area.

The transferred energy $W_{i,j}$ to the lubricated area at each grid point is calculated according to Eq. (7), using the averaged local force $\overline{F}_{i,j}$ between two consecutive steps of time for integration purposes. $v_{i,j}$ is the corresponding change in the local film thickness for the grid element (i,j). In the integral of Eq. (7), the product $v_{i,j}dt$ can be replaced with $\mathrm{d}h_{i,j}$, thus:

$$W_{i,j} = \int_{t_1}^{t_2} \overline{F}_{i,j} v_{i,j} \mathrm{d}t = \int_{h_1}^{h_2} \overline{F}_{i,j} \mathrm{d}h_{i,j} = \overline{F}_{i,j}(h_{2i,j} - h_{1i,j}) \tag{7}$$

The film shape and the corresponding pressure distribution are shown in Fig. 6 for a time step of the simulation. As can be seen, the contact pressure and the conjunctional film can be obtained simultaneously for the piston skirt-liner contact at the TS and the ATS. Consequently, energy transfer occurs at both sides of the partially skirted piston. The impact energy calculations are implemented accordingly. The lubricant film pressure is either positive or diminishes during an engine cycle. This in effect means that any cavitation is ignored in the current analysis as a full film is assumed within the conjunction. In other words, if the lubricant film is locally squeezed; $\mathrm{d}h < 0$, then $W_{i,j}$ takes a positive value and the oil film absorbs the impact energy (shown as Energy in Fig. 6). Otherwise, the energy is consumed in deforming the piston skirt or result in the rigid body motion of the piston away from the cylinder wall (shown as Null). It is assumed that the localised deformation energy does not contribute to noise propagation.

5. Structural attenuation of sound propagation

The energy transfer pattern from the piston skirt can be converted into impact power, P_v, by using the data of two successive time steps. The acoustic power of the engine block surface is required to estimate the radiated noise levels. Therefore, the structural attenuation ratio $(\eta_{a/v})$ is used to predict the sound power loss through the engine block structure. Structural attenuation is the ratio of acoustic power, P_a, at the outer surface of the engine block to impact power, P_v, at the inner surface of the cylinder liner [11]:

$$\eta_{\frac{a}{v}} = \frac{P_a}{P_v} \tag{8}$$

The acoustic power is usually expressed as a function of the surface vibration velocity v_r [18]:

$$P_a = \sigma \rho_a c_a A_r v_r^2 \tag{9}$$

Subscripts v and r refer to the impacted and radiating structures. σ is the surface radiation efficiency (varying between 0 and 1). For metallic parts vibrating at high frequencies, σ approaches unity [11]. ρ_a and c_a are the air density and wave propagation speed in air, respectively. A_r is the noise radiating surface area. The only unknown in Eq. (9) is the surface vibration velocity (v_r), defined below. The impact power can be expressed in terms of impact impedance Z and impact velocity v_v, using Eq. (10). The impact impedance is the inverse of impact mobility Y, which expresses the relationship between the excitation and response as [31]:

$$P_v = Z v_v^2 = \frac{v_v^2}{Y} \tag{10}$$

Thus, the attenuation factor can be rewritten by substituting Eq. (9) and Eq. (10) into Eq. (8), yielding:

$$\eta_{\frac{a}{v}} = \frac{\sigma \rho_a c_a A_r v_r^2}{Z v_v^2} \tag{11}$$

Table 1
Specifications of the Honda CRF 450 engine.

Engine specifications	Values
No. of cylinders	1
Fuel	Gasoline
No. of strokes	4
Cooling system	Water
Bore size	96 mm
Stroke	62.1 mm
Density of cylinder	2800 kg/m^3
Density of block	2753 kg/m^3
Wave speed in cylinder	5042 m/s
Average outside diameter of cylinder liner	106.5 mm
Average diameter of block	138.5 mm

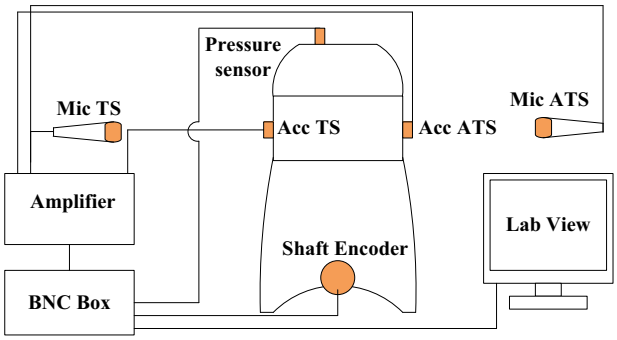

Fig. 7. The experimental set up used in the study.

In order to calculate the surface vibration velocity, a common assumption in the literature is that the impact energy is not dissipated whilst travelling through the engine block [11]. Conservation of energy between the impacted structure (cylinder liner) and the radiating structure (engine block) means:

$$\frac{1}{2}\rho_v h_{t,v} A_v v_v^2 = \frac{1}{2}\rho_r h_{t,r} A_r v_r^2 \tag{12}$$

Hence, the surface vibration velocity directly corresponds to the impact velocity. ρ, h_t and A are density, thickness and the surface area of the structure. Substitution of Eq. (12) into Eq. (11) yields the power attenuation factor in the form of Eq. (13), which is then calculated for every grid point (i,j) (equivalent to that of the conjunctional local lubricant film thickness), thus:

$$\left(\eta_{a/v}\right)_{i,j} = \frac{\sigma \rho_a c_a \rho_v h_{t,v}}{\rho_r h_{t,r}} \frac{(A_v)_{i,j}}{Z_{i,j}} \tag{13}$$

The cylinder liner directly interacts with the lubricant. Hence, the impact force should be determined using the lubricant film response. In Reynolds equation, it is assumed that the pressure gradient is constant through the thickness of the lubricant film [5]. As a result, the impact force, velocity and energy distributions follow the lubricant film shape. The impact impedance for the cylinder liner at each grid point, $Z_{i,j}$, is calculated by using the impact force and velocity distributions, employing Eq. (14) [31]:

$$Z_{i,j} = \frac{(F_v)_{i,j}}{(v_v)_{i,j}} \tag{14}$$

The attenuation factor $\left(\eta_{a/v}\right)_{i,j}$ at each grid point is calculated for both the TS and ATS surfaces, using Eqs. (13) and (14). The next step is to convert the local acoustic power at any chosen location to the equivalent sound pressure level. This is performed for correlation purposes with the experimentally obtained noise levels. The sound power levels from the engine surface can be estimated, using Eq. (15). P_{ref} is the reference power, equal to 10^{-12} W [32]:

$$(L_w)_{i,j} = 10 \log\left(\frac{(P_a)_{i,j}}{P_{\text{ref}}}\right) \tag{15}$$

Therefore, using Eq. (15), the sound power levels $(L_w)_{i,j}$ at the TS and ATS surfaces are calculated. The combination of noise radiation from both sides is received at any chosen spatial location. Initially, the local sound pressure levels (SPL) are

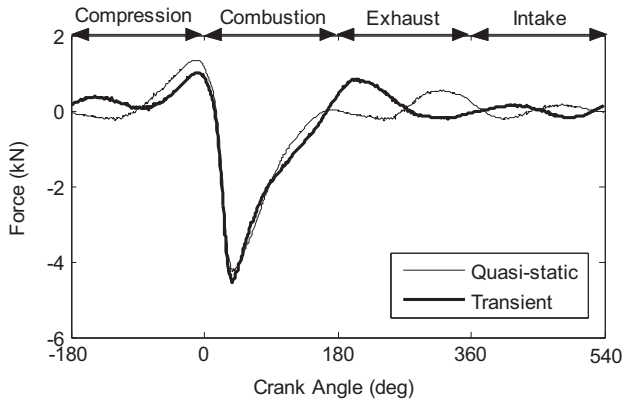

Fig. 8. Kinematic and inertial dynamic lateral force profiles vs. crank angle (nominal case).

transferred to any chosen location using Eq. (16). $\bar{s}_0$ is the acoustic field characteristics. If the engine is located in a free-field, then $\bar{s}_0 = 1$ and if the acoustic field is assumed to be semi-spherical, then $\bar{s}_0 = 2$. The latter case has been applied in this study. R_b is the distance from the block surface, thus [31]:

$$\mathrm{SPL}_{i,j} = (L_w)_{i,j} + 10\log\left(\frac{\bar{s}_0}{4\pi R_b^2}\right) \tag{16}$$

SPL values for the TS and ATS are combined using Eq. (17). SPL_T is the total sound pressure level at any location of interest [32], suitable for comparison purposes with the experimentally measured noise levels as

$$\mathrm{SPL}_T = 10\log\left(\sum_i\sum_j 10^{(\mathrm{SPL_{TS}})_{i,j}/10} + \sum_i\sum_j 10^{(\mathrm{SPL_{ATS}})_{i,j}/10}\right) \tag{17}$$

6. Experimental investigation

The experimental setup used for validating the proposed methodology is briefly explained here. More detailed information can be found in Littlefair et al. [24]. A Honda CRF 450R single-cylinder, 4-stroke motorbike SI engine is utilised (engine specifications are provided in Table 1). The experimental set up is shown in Fig. 7. The engine is resisted by an Oswald 250 kW transient dynamometer and controlled to the desired speeds. The exhaust fume is driven out through a ventilation fan. The in-cylinder pressure is measured using a Kistler spark-plug type pressure sensor. Two accelerometers are attached to the TS and ATS of the engine block to monitor surface vibrations. The TS and ATS noise levels are measured at 1 m distance from the block surface using microphones. An optical shaft encoder provides the corresponding crank angle to synchronise with the acquired noise signals. The data acquisition is implemented in the environment of LabVIEW.

7. Signal processing

Different sources inside and outside the engine block contribute to the monitored noise (such as valves, gears, bearings, the dynamometer and the test-cell air conditioning system). Signal post-processing is a common means to filter out the contributions of minor interest [31,33,34]. The operating frequencies of these events along with those of the piston impacts have been evaluated in these previous studies. The mechanical noise content is claimed to lie in the frequency range of 400–3200 Hz [31]. Other researchers have reported mechanical noise contributions to reside in the range: 1000–3000 Hz [35] or within 500–2000 Hz [36]. In the current study, the signal bandwidth was set at 450–3500 Hz, based on the aforementioned published work. The engine is installed in the test-cell, which is isolated from the outside environment to prevent interference. Nevertheless, the dynamometer and ventilation fan inside the test-cell introduce some uncertainties in the measurements. It is not possible to measure the contribution of these background sources directly as they operate concurrently with a running engine. However, the filtered signals were successfully matched to the mechanical events, as the presentation of the results demonstrates in the following section.

In the presence of the above uncertainty and the likelihood of low signal to noise ratio (SNR), the essential information contained in the signal can be extracted using time-frequency signal processing techniques in order to link the events observed in the signal to their excitation source [36]. The continuous wavelet transform (CWT) is a well-established method for time-frequency analysis of small oscillations that are highly localized in time, whereas the Fourier transform omits all time-localised information [37]. Therefore, CWT is applied to the highly transient nonlinear dynamics of the piston impact

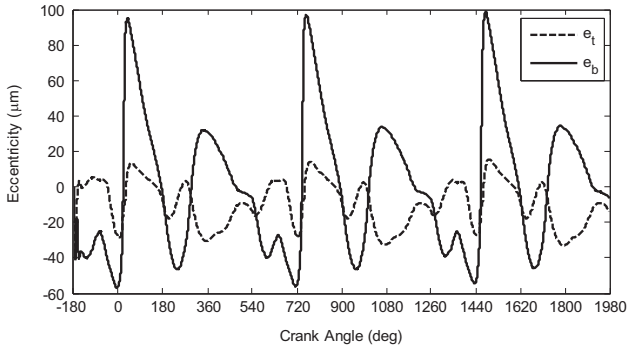

Fig. 9. Eccentricity at the top and bottom of the piston skirt vs. crank angle (nominal case).

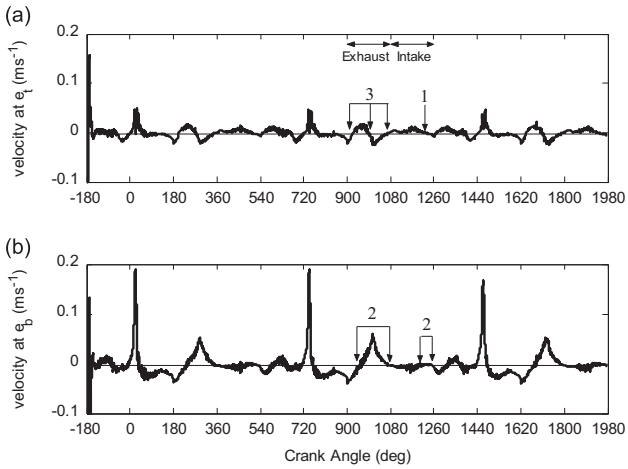

Fig. 10. Eccentricity velocity at: (a) the top and (b) bottom of the piston skirt (nominal case).

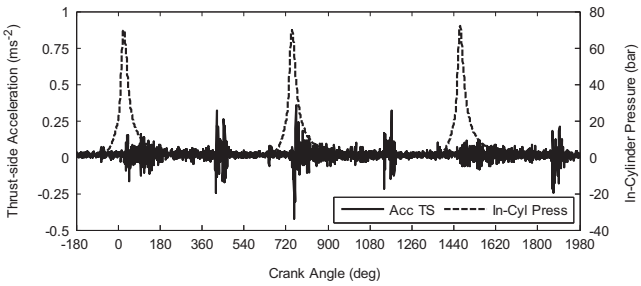

Fig. 11. Measured vibration acceleration at the engine block surface and correlation with the in-cylinder pressure (nominal case).

in this paper. The CWT function of Eq. (18) is used in the AutoSignal software environment for the current work [38]:

$$W_n(s) = \sum_{n'=0}^{N-1} x_{n'} \sqrt{\left(\frac{\delta t}{s'}\right)}\, \Psi_0^* \left[\frac{(n'-n)\delta t}{s'}\right] \tag{18}$$

The Ψ_0 function is the mother wavelet used in the CWT. The $(*)$ refers to the complex conjugate of the function. N is the data series length and n is an index of the localised time. s' is the wavelet scale and δt is the sampling interval. $x_{n'}$ represents the data series on which the CWT is based. The Morlet function is the most commonly used mother wavelet and it is applied to the current problem as [38]:

$$\Psi_0(\tau) = \pi^{-(1/4)} e^{im\tau} e^{-\tau^2/2} \tag{19}$$

m and τ are the wavenumber and the non-dimensional time parameter, respectively. The CWT parameters are set to return the best possible comparison between the experimental measurements and the analytical simulations for transient

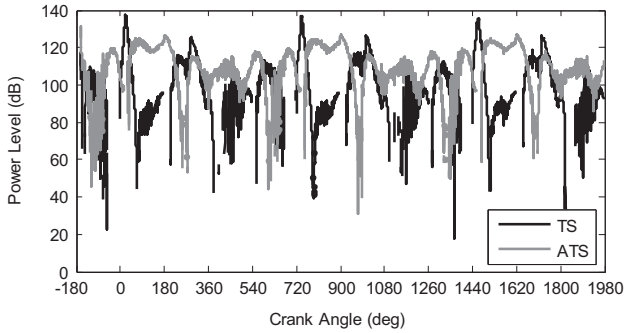

Fig. 12. Calculated sound power levels at the TS and ATS of the engine block (nominal case).

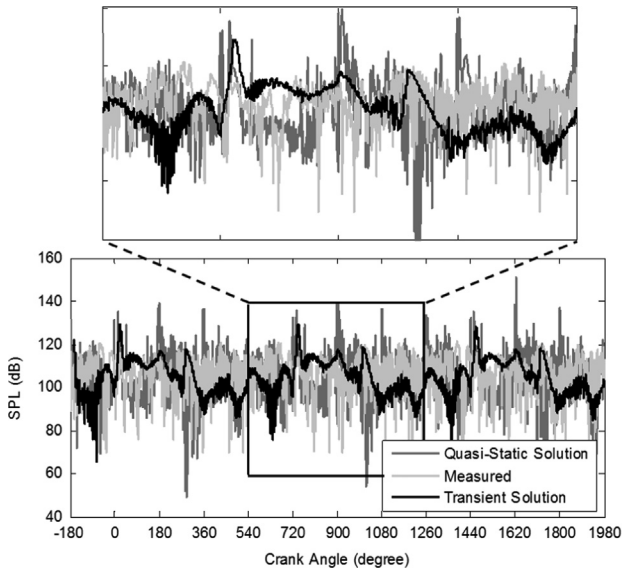

Fig. 13. Comparison of TS SPL measured and numerical data (nominal case).

problems. The adjustable parameters in the AutoSignal environment are m, n and the plot gradient. m and n equal 8 and 35 as default. The dB format is used with 21 dB value for the gradient.

8. Results and discussion

Experimental measurements were made at two different engine conditions: (i) 3500 rpm and 40 Nm and (ii) 4250 rpm and 42 Nm. Those test conditions are used to show the generic nature of the numerical predictive model through validation with the measured data. Transient numerical solutions of the piston's secondary motion were carried out for both the aforementioned test conditions. A kinematic quasi-static solution (excluding the effects of piston pin rotation and lubricant film squeeze effect) was carried out for the case of 3500 rpm engine speed only in order to study the validity of the approach against the full transient analysis.

8.1. 3500 rpm engine speed and 40 Nm torque (nominal case)

Since the lateral force is an indication of potential ensuing piston slap, an investigation of the resultant side force obtained from the quasi-static or transient inertial dynamics approaches is necessary. Fig. 8 shows a comparison of two net side force plots (one through quasi-static and the other through transient dynamics analysis). These are for an engine cycle at the engine speed of 3500 rpm with a maximum torque output of 40 Nm. The negative force values indicate net force direction towards the thrust side (TS) whilst the positive values correspond to the net force direction towards the anti-thrust side (ATS). The gas force is dominant from the end of the compression stroke up to 180° crank angle position in the power stroke. In this interval, the lateral (side) force for both the kinematic and the inertial dynamics analyses remain in agreement. In the other parts of the engine cycle, the inertial forces are dominant, thus there is some deviation between the results of the transient inertial dynamics and that of quasi-statics. This deviation may be the result of piston tilt about the

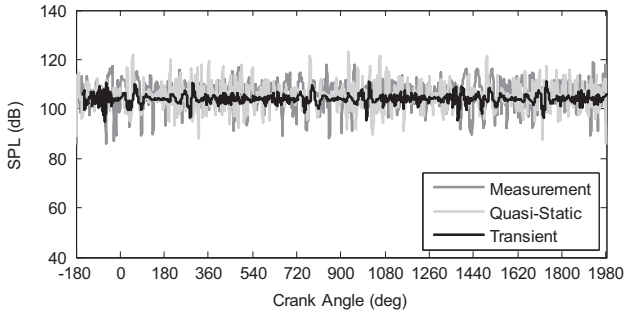

Fig. 14. Filtered SPL histories as a function of crank angle (3500 rpm and 40 Nm).

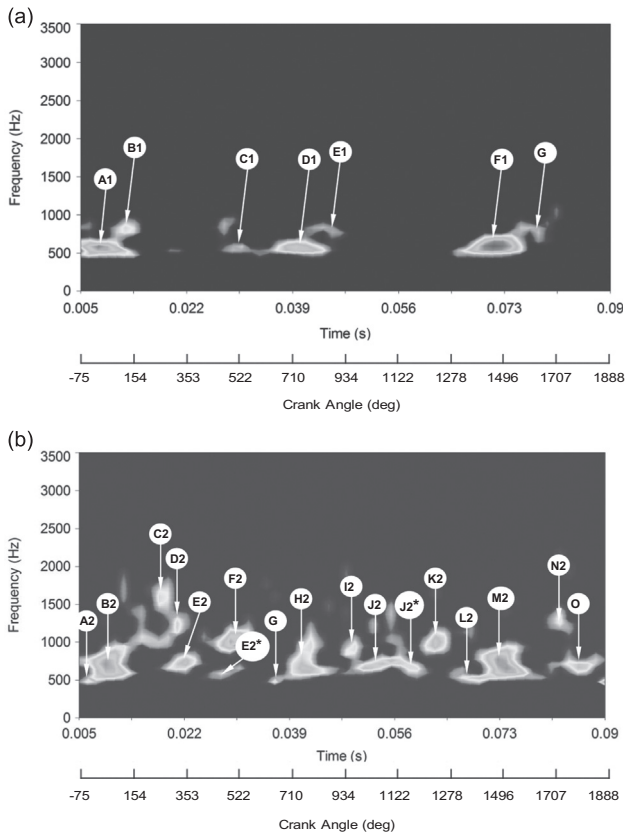

Fig. 15. The Continuous Wavelet Spectra (CWS) of the noise for three consecutive engine cycles (nominal case): (a) TS and (b) ATS.

pin-bore bearing. In both analyses, six instances of incursion from the piston axis occur, which are indicated by the lateral force plots crossing the zero net force. Hence, six piston slaps can potentially occur [33,34].

Monitoring piston eccentricities (at its top and bottom skirt surfaces) is useful when investigating its tilting motion. Eccentricity plots obtained from the transient model are presented in Fig. 9 for the top and bottom of the skirt (i.e. e_t and e_b, respectively) for three consecutive engine cycles. The top (e_t) and bottom (e_b) eccentricities are the deviation of the piston top and bottom from its centre-line axis, respectively. The results for the first 20° crank angle are ignored, since the squeeze film action is initially neglected for sake of numerical stability. The largest eccentricity values are noted at the bottom of the piston skirt during the power stroke and around the bottom-dead-centre (BDC) during the exhaust stroke. Larger eccentricities can lead to higher piston lateral velocities and potentially a greater degree of impact severity. The repetitive nature of piston secondary dynamics is clear for the three cycles shown in the figure.

The approaching velocities at the top, $\dot{e}_t$, and bottom, $\dot{e}_b$, of the skirt are presented in Fig. 10. As expected, velocity amplitudes are higher at the bottom of the skirt, where the observed displacements are larger. When the approach velocity diminishes, either an impact has occurred or there may simply be no net side force (no secondary piston dynamics: momentary equilibrium condition). Therefore, identifying piston slap through the use of rates of change of top and bottom skirt eccentricities (lateral velocities) carries a certain degree of uncertainty. Thus, the velocities $\dot{e}_t$ and $\dot{e}_b$ are compared with

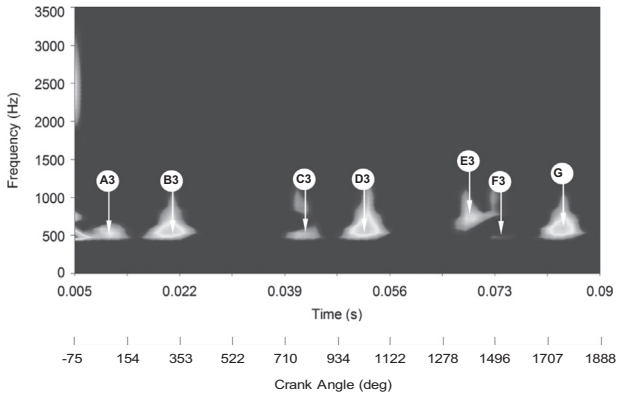

Fig. 16. Transient numerical CWS for three consecutive engine cycles (nominal case).

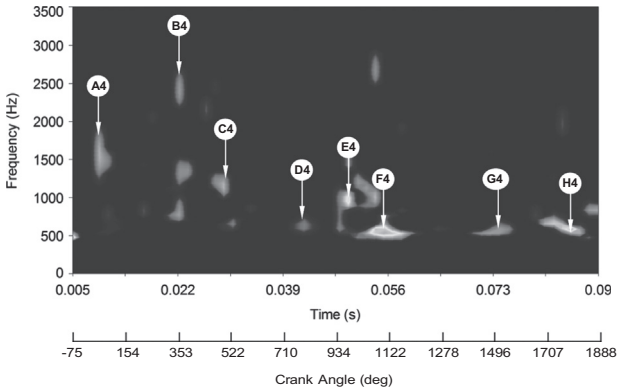

Fig. 17. Quasi-static numerical CWS for three consecutive engine cycles (nominal case).

the raw measured surface acceleration data at the thrust side (Fig. 11). The acquired acceleration signals are qualitatively repeatable. However, their amplitudes can be inconsistent for similar observed events. This characteristic is mostly noted during the power stroke, where the combustion pressure reaches its maximum value. Close observation of the gas pressure has revealed that the engine knock due to uneven gas detonation is a possible source of this lack of consistency, particularly for the inherently unbalanced single cylinder configuration [39].

The second engine cycle has been chosen to examine the behaviour of the approach velocities (between 540° and 1260° crank angles). At least two momentary stationary points (zero velocity positions) are present between the crank angles 540° and 720°, whilst a significant spike occurs in the corresponding measured acceleration signal (acceleration reaches its maximum value with zero velocity). For $\dot{e}_t = 0$, the zero-value locations marked 3 and 1 are present during the exhaust and intake strokes, respectively. The location of such events changes to those marked as 2 and 2 for $\dot{e}_b = 0$ (Fig. 10). This difference is attributed to the sense of tilt of the piston. In the exhaust stroke the impact signature is masked by the neighbouring accelerations and it cannot be easily discerned (Fig. 11). Therefore, the uncertainties encountered with $\dot{e}_t$ and $\dot{e}_b$ make it difficult to predict the piston slap events. Further refinement would be required both for the numerical method, as well as the experimental measurements, which are described in the following sections.

The most significant output of the proposed method is the radiated power from the vibrating engine block surface. This is presented in Fig. 12 for three consecutive engine cycles. The darker trace corresponds to the thrust side (TS) and the grey trace relates to the anti-thrust side (ATS). The results for the first 20° crank angle are again discounted. There are some gaps in the traces of Fig. 12, where no power levels have been plotted. At these instances, the theoretical calculations encounter numerical instabilities and therefore the data is omitted. These instabilities are the result of instantaneously non-varying lubricant film thickness, where no impact power is transferred onto the block. The maximum power is radiated during the combustion stroke, exhibiting a repeatable pattern in all the engine cycles. Fig. 12 indirectly represents the direction of piston slap to the cylinder liner, when taking into account the level of sound power emanating from the TS and the ATS. The TS and ATS sound power levels are calculated separately and can be treated as two distinct noise sources. In practice, the experimentally obtained sound power levels are the combination of both sources, occurring simultaneously. The combined sound power level alters with direction as the distance from each source varies with respect to the position of the receiver. Therefore, there are differences between the combined and single source sound power levels at the TS, since the former includes the effects of both the TS and the ATS sources (determined at the TS measurement location). It is well-established in the literature that the most severe impacts prevail at the TS during combustion. However, during other periods of the

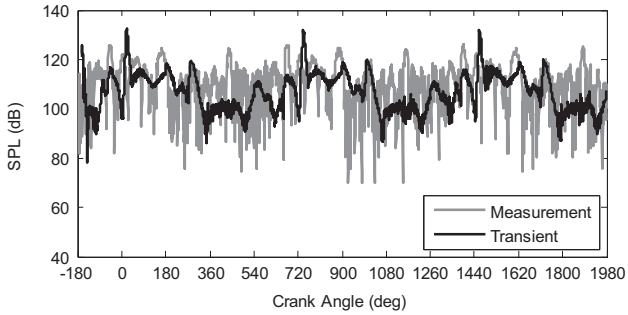

Fig. 18. Transient SPL for three consecutive engine cycles (4250 rpm and 42 Nm).

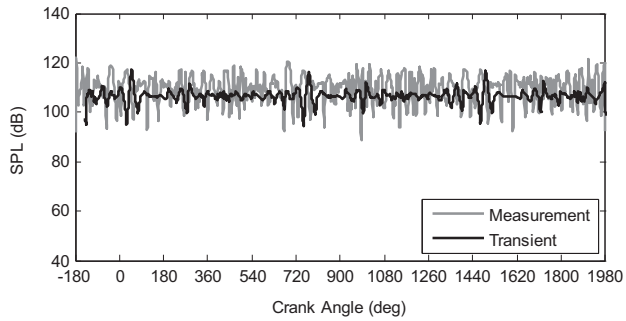

Fig. 19. Filtered SPL histories as a function of crank angle for three consecutive engine cycles (4250 rpm and 42 Nm).

engine cycle, the ATS power levels can equal or surpass those from the TS. The severity of power/sound levels depends on the location and energy of the piston inside the clearance. For instance, the piston impinges at the TS wall at the beginning of the combustion stroke, where a severe side force acts for a short duration. The ATS wall transfers higher power as the piston separates from the TS wall towards the end of the combustion stroke.

The sound pressure level (SPL) is calculated at a distance of 1 m from the TS (Fig. 13) and it is compared with the measured noise levels. Although the combined TS and ATS SPL data can exhibit different characteristics (since their power levels and directions differ), only the combined predicted TS results are presented for the sake of brevity. Therefore, hereinafter all the combined SPLs for transient and quasi-static solutions refer to the TS location. The three plots in Fig. 13 generally conform well. To provide a clearer view, the results are magnified for the second engine cycle in the inset to the figure. The theoretical results relate to the piston–cylinder liner interactions only. However, measurements include contributions from all noise sources in and out of the engine block. Consequently, the measured noise levels exceed those predicted during the intake and compression strokes, where the contributions of other sources become comparable to the piston slap as the gas pressure is reduced. Furthermore, in the transient dynamics solution the inertial effect of components other than the piston are neglected and the extent of deviation in the estimation of noise levels is anticipated (over-estimation or under-estimation). Therefore, the experimental and simulated noise signals have been filtered using the frequency interval (450–3500 Hz) chosen in section 7. The resulting time histories are shown in Fig. 14. The three signals compare well with the anticipated average noise level of 106.04 dB for the measurements, and 104.05 dB and 105.26 dB for the transient dynamics and quasi-static predictions respectively. Although both analytical models agree well with the measurements, further analysis would be required to assess which is the most accurate model in terms of highlighting the piston slapping events.

In order to identify the highest energy contributions in the acquired signals, two-dimensional Continuous Wavelet Spectra (CWS) are presented (using the AutoSIGNAL software). The spectra corresponding to the measured noise at the TS and ATS (at 1 m distance) are shown in Fig. 15. The main contributions occur at 0.0082 s (A1), 0.04 s (D1), and 0.0713 s (F1) in the TS spectrum with additional less significant events at about 0.012 s (B1), 0.0305 s (C1), 0.0467 s (E1) and 0.0784 s (G1). The same main contributions are also present in the ATS spectrum around 0.00925 s (B2), 0.041 s (H2), and 0.073 s (M2). Additional contributions are identified in the ATS spectrum, which are located at 0.006 s (A2), 0.018 s (C2), 0.0205 s (D2), 0.022 s (E2), 0.0248 s (E2*) and 0.0303 s (F2) for the first engine cycle, at 0.037 s (G2), 0.049 s (I2), 0.050 s (J2) and 0.0625 s (K2) for the second engine cycle and finally at 0.068 s (L2), 0.0828 s (N2) and 0.0861 s (O2) for the third engine cycle. These contributions follow the same pattern in all the displayed cycles. The highest energy contributions are located in the frequency band 500–1500 Hz. As described earlier, the experimental measurements are the result of combined sources (at the TS and ATS). Therefore, TS events can be present in the ATS location measurements with similar severity. The events D1 and H2 represent this behaviour in Fig. 15.

The CWS of the transient numerical results are presented in Fig. 16 for the combined SPL. Two predicted events are present in each cycle which can be correlated to those measured (in a temporal, as well as a spectral sense). These occur at 0.0107 s (A3) and 0.0203 s (B3) for the first cycle, at 0.0419 s (C3) and 0.0524 s (D3) for the second cycle and finally at 0.0688 s (E3), 0.0729 s (F3) and 0.08146 s (G3) in the third cycle. A3, B3, C3, D3, F3 and G3 correspond to B2, E2, H2, J2, M2 and O2 (measured data) respectively. The contribution labelled F3 is rather weak and can be attributed to the fluctuations in the in-cylinder pressure between different cycles (cycle-to-cycle combustion variation). Fig. 17 corresponds to the quasi-static CWS. As can be seen, good agreement is observed after 0.039 s between the quasi-static and measured spectra (the latter events occur around 0.043 s (D4), 0.049 s (E4), 0.055 s (F4), 0.072 s (G4) and 0.0828 s (H4)). Prior to this time juncture, there are mismatched events (either temporally or based on spectral contributions). For instance the events marked as A4, B4 and C4 are approximately equivalent to B2, E2 and F2 temporally. However, their spectral compositions do not coincide.

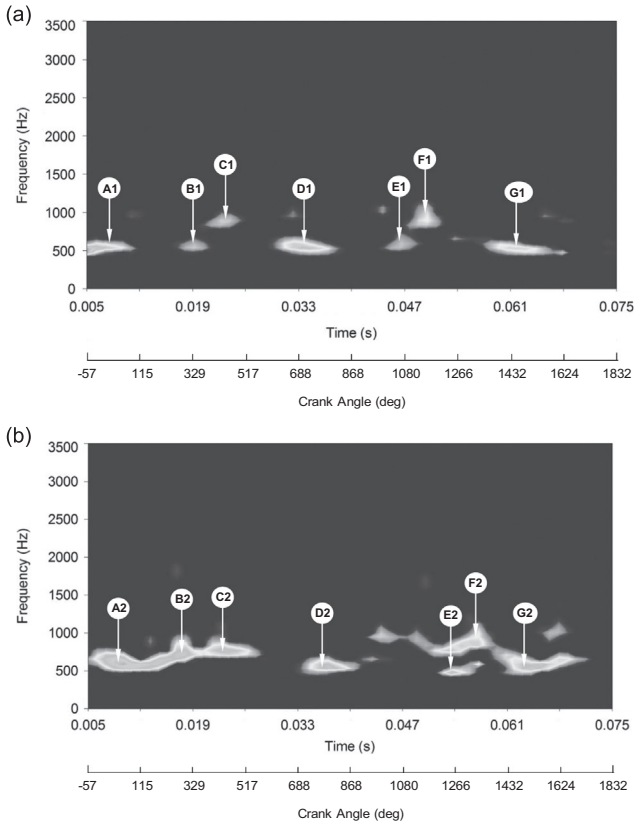

Fig. 20. CWS of the noise for three consecutive engine cycles (4250 rpm and 42 Nm): (a) TS and (b) ATS.

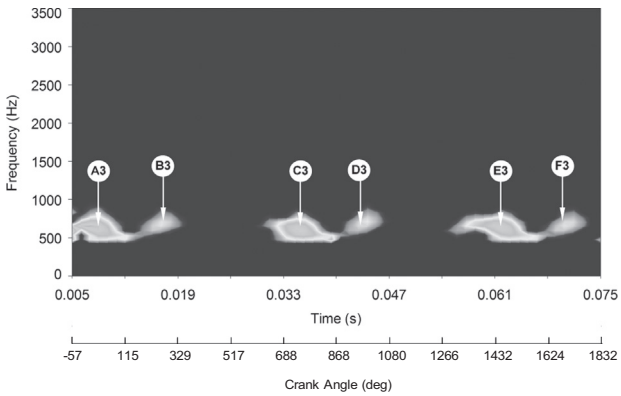

Fig. 21. Transient numerical CWS for three consecutive engine cycles (4250 rpm and 42 Nm)

Overall, the transient approach is more consistent in predicting repeatable events and their degree of severity. Therefore, hereinafter the accuracy of the transient dynamics' predictions is only assessed for the remaining test case at the engine speed of 4250 rpm.

Small deviations in noise levels may be expected in the transient results due to the omission of some inertial parameters, such as the connecting rod inertia, bearings and the crankshaft. These deviations can influence the severity of the predicted responses. As a consequence, some difference in the number of events can be observed between the measurements and the transient dynamics' predictions. Furthermore, the selected frequency interval might include noises from other mechanical sources, which produce events in the same frequency range. Valve opening and closure impacts can possibly coincide with piston slaps. The inlet valve closure (IVC) occurs at about 50° crank angle position or immediately after bottom dead centre (ABDC) in the compression stroke. The exhaust valve opens (EVO) at 55° crank angle or immediately before bottom dead centre (BBDC) in the combustion stroke. At the crank angle of 15° or slightly thereafter the inlet valve opens (IVO) in the exhaust stroke. Exhaust valve closure (EVC) commences at approximately the crank angle of 25° after top dead centre (ATDC). These locations can be correlated to B1, E1 and G1 for EVO, E2, J2 and O2 for IVO, E2∗ and J2∗ for EVC and A2, G2 and L2 for IVC.

8.2. 4250 rpm engine speed and 42 Nm input torque

Fig. 18 depicts the noise levels from the experimental measurements and the corresponding numerical predictions using the transient dynamics analysis at the engine speed of 4250 rpm. The predictions conform well to the experimental measurements for the power and exhaust strokes. In the other engine strokes, the measurements exhibit slightly higher SPL values. Filtering is applied to both the experimental signal and numerical response, the outcome of which is shown in Fig. 19. The average noise level for the measured data is 109.45 dB, whereas that for the predictions is 106.59 dB. As expected, the increase in engine speed leads to increased noise level, with the mean noise levels having increased by approximately 3 dB compared with the 3500 rpm engine speed case.

Graphical interpretations of the piston slap events and their dominant frequencies are shown in the CWS of the TS and the ATS measurements (Fig. 20). At the TS, six significant events are evident in the first two engine cycles at 0.0077 s (A1), 0.0183 s (B1), 0.023 s (C1), 0.033 s (D1), 0.047 s (E1), and 0.05 s (F1). In the last engine cycle, only one major event is noted around 0.061 s (G1). There are other events in the ATS spectrum around 0.0095 s (A2), 0.0173 s (B2), 0.0229 s (C2), 0.0365 (D2), 0.0534 (E2), 0.0563 (F2) and 0.0636 s (G2). The spectrum of the corresponding transient numerical predictions is shown in Fig. 21. The first two events occur around 0.0077 s (A3) and 0.0168 s (B3), matching those measured (Fig. 20). More events take place at 0.035 s (C3), 0.044 s (D3), 0.0616 s (E3) and 0.07 s (F3). The first and third events occur simultaneously at both the TS and the ATS, whilst the event marked by (D3) is only observed in the TS spectrum. The event (G2) extends in the ATS spectrum, showing the same characteristics as (F3). The CWS for the measured TS and ATS reveals three main piston events per engine cycle, whilst in the numerical results only two such events are present per engine cycle. This difference can be attributed to the omission of inertial parameters other than the piston inertia (e.g. pin, connecting rod) which may affect the timing of the events. A comparison between the recorded events and the valve timing reveals that piston slap can coincide with the valve-induced events at 0.023 s (C1), 0.05 s (F1) and 0.0563 s (F2). Small contributions are also present at 1000 Hz (in the TS spectrum), which are also correlated to the valve events. However, as the engine speed increases, the valve events become less apparent.

9. Conclusions

A new analytical/numerical method is presented for the estimation of IC engine piston slap events, correlating the piston secondary motion to the surface vibrations of the engine cylinder. The estimated acoustic power is converted into sound pressure levels at any desired location in the vicinity of the engine. The method proposed is able to successfully predict the time of piston slap events during the engine cycle, as well as their associated frequencies. It also provides a reasonable estimate of engine noise levels arising from piston slap events. The main contribution of the paper is in the coupling of transient dynamics and impact through the lubricated piston-liner conjunction. An elastohydrodynamic regime of lubrication occurs at the TS and the ATS, yielding lubricant films which cushion the effect of piston slap, enabling determination of local mechanical impedances and the energy transferred to the liner. Two-dimensional continuous wavelets are then used to determine the integrity of the devised method through validation against measured noise from a fired single cylinder engine under a controlled test-cell protocol. The method can detect the amplification of noise levels as the engine speed increases in a more robust manner compared to a quasi-static approach. Further improvements can be made by inclusion of precise engine block geometry, piston assembly inertial elements and hysteretic structural damping. These constitute future directions of the current research.

Acknowledgement

The authors wish to express their gratitude to the EPSRC for the financial support extended to the Encyclopaedic Program Grant (EP/G012334/1), under which this research was carried out. Thanks are also due to the consortium of industrial partners of the Encyclopaedic project, particularly to Capricorn Automotive in this instance.

References

[1] B. S. Andersson, Company's perspective in vehicle tribology, *Proceedings of the 18th Leeds-Lyon Symposium*, Lyon, France, 3–6 September 1991, in: D. Dowson, C. M. Taylor and M. Godet, (Eds.), Elsevier, New York, pp. 503–506.
[2] H. Kanda, M. Okubo, T. Yonezawa, Analysis of noise sources and their transfer paths in diesel engines, SAE Technical Paper 900014, 1990, pp. 1 – 8.
[3] M. Okubo, H. Kanda, T. Yonezawa, Analysis and reduction of piston slap noise in diesel engines, SAE Technical Paper 890127 (1989).
[4] R. DeJong, N. Parsons, Piston slap noise reduction in a vee-block diesel engine, SAE Technical Paper 820240 (1982).
[5] R. Gohar, H. Rahnejat, *Fundamentals of Tribology*, Imperial College Press, London, 2008.
[6] P. McFadden, S. Turnbull, Dynamic analysis of piston secondary motion in an internal combustion engine under non-lubricated and fully flooded lubricated conditions, *Proceedings of the Institution of Mechanical Engineers, Part C: Journal of Mechanical Engineering Science* 225 (11) (2011) 2575–2585, http://dx.doi.org/10.1177/0954406211408674.
[7] E. Abu Nada, I. Al-Hinti, B. Akash, A. Al-Sarkhi, Thermodynamic analysis of spark ignition engine using a gas mixture model for the working fluid, *International Journal of Energy Research* 31 (11) (2007) 1031–1046.
[8] V. D' Agostino, D. Guida, A. Ruggiero, C. Russo. Optimized EHL piston dynamics computer code, *Proceedings of the 5th International Conference on Tribology*, AITC-AIT, Parma, September 2006, pp. 9.
[9] S. Ge-qun, W. Hai-qiao, H. Rui, The transfer function of combustion noise in DI-diesel engine, SAE Technical Paper 2005-01-2486, 2005.
[10] N. Lalor, E. Grover, T. Priede, Engine noise due to mechanical impacts at pistons and bearings, SAE Technical paper 800402, 1980.
[11] E.E. Ungar, D. Ross, Vibrations and noise due to piston-slap in reciprocating machinery, *Journal of Sound and Vibration* 2 (2) (1965) 132–146.
[12] S.H. Cho, S.T. Ahn, Y.H. Kim, A simple model to estimate the impact force induced by piston slap, *Journal of Sound and Vibration* 255 (2) (2002) 229–242.
[13] M. Kushwaha, S. Gupta, P. Kelly, H. Rahnejat, Elasto-multi-body dynamics of multi-cylinder internal combustion engine, *Proceedings of Institution of Mechanical Engineers, Part K: Journal of Multi-body Dynamics* 216 (4) (2002) 281–293.
[14] H. Murakami, N. Nakanishi, N. Ono, T. Kawano, New three-dimensional piston secondary motion analysis method coupling structure analysis and multi body dynamics analysis, *SAE International Journal of Engines* 5 (1) (2011) 42–50.
[15] M. Perera, S. Theodossiades, H. Rahnejat, Elasto-multi-body dynamics of internal combustion engines with tribological conjunctions, *Proceedings of Institution of Mechanical Engineers, Part K: Journal of Multi-body Dynamics* 224 (3) (2010) 261–277.
[16] M. Perera, S. Theodossiades, H. Rahnejat, A multi-physics multi-scale approach in engine design analysis, *Proceedings of Institute of Mechanical Engineers, Part K: Journal of Multi-body Dynamics* 221 (3) (2007) 335–348.
[17] D.F. Li, S.M. Rohde, H.A. Ezzat, An automotive piston lubrication model, *ASLE Transactions* 26 (2) (1983) 151–160.
[18] K. Ohta, K. Amano, A. Hayashida, G. Zheng, Analysis of piston slap induced noise and vibration of internal combustion engine, *Journal of Environment and Engineering* 6 (3) (2011) 712–722.
[19] S. Gerges, J. de Luca, N. Lalor, Effect of cylinder lubrication on piston slap, SAE Technical Paper 2005-01-2165, 2005.
[20] T. Nakada, A. Yamamoto, T. Abe, A numerical approach for piston secondary motion analysis and its application to the piston related noise, SAE Technical Paper 972043, 1997, pp. 1361 – 1370.
[21] S. Balakrishnan, H. Rahnejat, Isothermal analysis of piston skirt-to-cylinder wall contacts under combined axial, lateral and tilting motion, *Journal of Physics, Part D: Applied Physics* 38 (5) (2005) 787–799.
[22] J. Cho, S. Moon, A numerical analysis of the interaction between the piston oil film and the component deformation in a reciprocating compressor, *Tribology International* 38 (5) (2005) 459–468.
[23] F. McClure, *Numerical Modeling of Piston Secondary Motion and Skirt Lubrication in Internal Combustion Engines* PhD Thesis, Massachusetts Institute of Technology, 2007 USA.
[24] B. Littlefair, M. De la Cruz, S. Theodossiades, R. Mills, Transient tribo-dynamics of thermo-elastic compliant high-performance piston skirts, *Tribology Letters* 53 (1) (2014) 51–70.
[25] B. Littlefair, M. De La Cruz, R. Mills, S. Theodossiades, Lubrication of a flexible piston skirt conjunction subjected to thermo-elastic deformation: a combined numerical and experimental investigation, *Proceedings of Institute of Mechanical Engineers, Part J: Journal of Engineering Tribology* 228 (1) (2014) 69–81.
[26] N. Dolatabadi, S. Theodossiades, S.J. Rothberg, On the identification of piston slap events in internal combustion engines using tribodynamic analysis, *Journal of Mechanical Systems and Signal Processing* 58 – 59 (2015) 308–324.
[27] J. Cho, Effects of skirt profiles on the piston secondary movements by the lubrication behaviors, *International Journal of Automotive Technology* 5 (1) (2004) 23–31.
[28] D. Dowson, G. Higginson, A numerical solution to the elasto-hydrodynamic problem, *Journal of Mechanical Engineering Science* 1 (1) (1959) 6–15.
[29] N. Morris, R. Rahmani, H. Rahnejat, P.D. King, B. Fitzsimons, Tribology of piston compression ring under transient thermal mixed regime of lubrication, *Tribology International* 59 (2013) 248–258.
[30] C. Roelands, *Correlational Aspects of the Viscosity – Temperature – Pressure Relationship of Lubricating Oils* PhD Thesis, Technical University Delft, 1966.
[31] F. Fahy, P. Gardonio, *Sound and Structural Vibration: Radiation, Transmission and Response*, Academic Press, Netherlands, 2007.
[32] C.E. Wilson, *Noise Control, Revised Edition*, Krieger Publishing Company, Malabar, Florida, USA, 2006.
[33] Z. Geng, J. Chen, Investigation into piston-slap-induced vibration for engine condition simulation and monitoring, *Journal of Sound and Vibration* 282 (3) (2005) 735–751.
[34] S.D. Haddad, K.T. Tian, An analytical study of offset piston and crankshaft designs and the effect of oil film on piston slap excitation in a diesel engine, *Mechanism and Machine Theory* 30 (2) (1995) 271–284.
[35] K. Ohta, Y. Irie, K. Yamamoto, H. Ishikawa, Piston slap induced noise and vibration of internal combustion engines (1st Report, Theoretical Analysis and Simulation), SAE Technical Paper 870990, 1987.
[36] K. Nakashima, Y. Yajima, K. Suzuki, Approach to minimization of piston slap force for noise reduction–investigation of piston slap force by numerical simulation, *JSAE Review* 20 (2) (1999) 211–216.
[37] M. Chiollaz, Engine noise characterisation with Winger – Ville time-frequency analysis, *Mechanical Systems and Signal Processing* 7 (5) (1993) 375–400.
[38] AutoSignal version 1.7 release notes, Sea Solve Software Inc., 1999 – 2003.
[39] H. Rahnejat, *Multi-body dynamics: vehicles, machines and mechanisms*, Professional Engineering Publishing, Bury St Edmunds, UK, 1998.